Blucher Mechanical Engineering Proceedings
May 2014, vol. 1 , num. 1
www.proceedings.blucher.com.br/evento/10wccm

10th World Congress on Computational Mechanics
8-13 July 2012 • São Paulo • Brazil

INFLUENCE OF HYDROSTATIC STRESS DISTRIBUTION ON THE MODELLING OF HYDROGEN ASSISTED STRESS CORROSION CRACK GROWTH

N. R. Raykar[1,2,3], S. K. Maiti[2], R. K. Singh Raman[3,4]

[1] IITB-Monash Research Academy, CSE Building, 2nd Floor, IIT Bombay, Powai, 400076, India (nilesh.raykar@iitb.ac.in)

[2] Department of Mechanical Engineering, IIT Bombay, Powai, 400076, India

[3] Department of Mechanical and Aerospace Engineering, Monash University, Clayton, VIC 3800, Australia

[4] Department of Chemical Engineering, Monash University, Clayton, VIC 3800, Australia

Abstract. *This study on stable crack growth under hydrogen assisted stress corrosion cracking (HASCC) is concerned with modelling of two interdependent processes: diffusion of hydrogen into material, and the resulting advancement at crack tip. The concentration of diffused hydrogen ahead of the crack tip is influenced by the local distribution of hydrostatic stresses and plastic strains. The influence of hydrostatic stress may become predominant at lower plastic strain levels for hydrogen distribution and crack growth but, to the best of authors' knowledge, this has not been substantiated. The present study deals with modelling of the interdependent processes and examines the issue.*

The crack growth has been studied in compact tension specimens of a structural steel under HASCC conditions at three levels of plastic strain. A hydrogen concentration dependent cohesive zone model (HCDCZM) has been employed. The distribution of diffused hydrogen is obtained by solving the governing non-linear equation of diffusion which includes the hydrostatic stress effect using a numerical scheme based on finite difference method. The hydrogen distribution is then used to predict crack propagation using a finite element based cohesive zone model.

This paper presents details of the modelling and results concerning the crack tip hydrogen concentration and comparison of predicted and experimental variation of crack opening displacement with crack extension. The influence of hydrostatic stress on the hydrogen distribution is noticeable for the two slower loading rates where plastic strain levels are below 0.05. For all three loading rates, the average hydrogen concentration near the crack tip is higher in the present study than the results obtained in an earlier study by excluding the effect of hydrostatic stress. This difference calls for a decrease in cohesive strength reduction factor to maintain an equal level of crack extension rate as in the earlier study. The results are acceptable without any need to change the effective diffusivity.

Keywords: *Modelling of hydrogen assisted stress corrosion cracking (HASCC), Cohesive zone modelling of HASCC, Effect of hydrostatic stress on HASCC.*

1. INTRODUCTION

Hydrogen assisted stress corrosion cracking (HASCC) is a term used to describe accelerated damage to material under combined action of tensile stress and corrosive environment containing hydrogen. The hydrogen could be available directly or as a product of corrosion reaction. The crack growth during HASCC is sudden and generally difficult to monitor in situ. The insidious nature of HASCC poses serious safety and operational challenges for core industries such as aviation, marine, and nuclear and fossil power. Avoidance and control of HASCC is an ongoing research topic; several methods have been developed over the years for establishing structural integrity in the HASCC regime. Some efforts have given rise to empirical formulae; some have given experimental databases and others have helped to evolve numerical methods. The development of numerical methods is based on mechanistic models of HASCC to study initiation and propagation of crack. These models are of two types [5]: some predict the threshold stress intensity factor K_{TH} below which no crack extension occurs and others estimate the stable crack growth rates $\frac{da}{dt}$. These models are useful in validating a design against failure and in predicting residual life of a component. This paper employs a model for studying $\frac{da}{dt}$ and characterising HASCC resistance of a material.

The models of HASCC deal with parameters which promote the damage and mechanisms that explain the underlying physical events and sequence of processes preceding the damage. The parameters promoting HASCC [5] may be categorised as follows. *(a)* Mechanical: load or stress intensity factor K, rate of application of load, sequence and cyclic frequency of load. *(b)* Metallurgical: yield strength which is typically governed by material microstructure, grain size, purity of material and diffusivity of material. *(c)* Chemical: concentration of hydrogen inside material, pressure of hydrogen or pH of environment, cathodic polarisation of aqueous media and temperature.

The experimental and theoretical work suggests that the mechanisms of HASCC are mainly three: hydrogen enhanced decohesion (HEDE), hydrogen enhanced localised plasticity (HELP) and adsorption induced dislocation emission (AIDE) [10]. The sequence of processes preceding the hydrogen induced cracking have been examined by Gangloff [5]. He has indicated these to include transport of reactants around crack tip, generation of hydrogen through chemical reaction, adsorption of hydrogen at crack face, inward diffusion of hydrogen to crack process zone and finally, damage and fracture of material. These multiple parameters, mechanisms and processes are difficult to be accommodated in a single model; the existing models account for a sub-set of these factors. The model used in the present study incorporates only rate of loading, diffusivity of material and concentration of hydrogen. Further it accommodates HEDE mechanism and two processes: diffusion and fracture.

A hydrogen concentration dependent cohesive zone model (HCDCZM) [12, 15, 16] is used here for modelling stable crack growth under HASCC which is dominated by HEDE mechanism. This mechanism assumes a decrease in cohesive strength of the bond between metal atoms due to the presence of solute hydrogen within metal lattice. The decrease in cohesive strength is considered proportionate to the local hydrogen concentration [9].

The HCDCZM utilises cohesive zone model (CZM) to handle fracture process. The CZM was introduced by Barenblatt [2] originally for study of crack growth in brittle materials and it was later adopted for modelling of fracture in metals. The CZM helps contain damage to the material during fracture process over a narrow zone close to the crack tip, through a traction separation law (TSL). The TSL defines a relationship between cohesive stress and separation within the atoms of metal lattice. The progressive damage to the load carrying capacity of material and subsequent formation of fracture surfaces occur within the narrow cohesive zone. The CZM allows simpler handling of the crack growth simulation as it avoids evaluation of singularity near the crack tip. The damage caused by the presence of hydrogen is included into CZM by a reduction in cohesive strength proportionate to the local hydrogen concentration.

The hydrogen distribution inside the material is determined by a numerical modelling of hydrogen transport by diffusion process. The source of hydrogen is typically a corrosion reaction promoted by agents in the environment. Typical anodic and cathodic corrosion reactions for iron in aqueous environments are as follows.

$$Fe = Fe^{2+} + 2e^{-} \qquad \text{(anodic partial reaction)}$$

$$2H^{+} + 2e^{-} = 2H(H_2) \qquad \text{(cathodic partial reaction for } pH < 7\text{)}$$

$$2H_2O + 2e^{-} = H_2 + 2OH^{-} \qquad \text{(cathodic partial reaction for } pH \geq 7\text{)}$$

A part of hydrogen atoms thus evolved near the crack tip combine with each other and escape as gas bubbles as they are too large to diffuse into metal lattice; however, some atoms enter into the metal and get driven towards the region near the crack tip under the influence of stress field. The hydrogen is considered to move inside the metal largely by normal interstitial lattice site (NILS) diffusion [17]. The movement of hydrogen through NILS is arrested at various micro-structural trap sites such as, voids, inclusions, grain boundaries, collectively termed as traps [18] where the hydrogen gets accumulated.

The approach of Oriani [13] for modelling of hydrogen diffusion assumes that the dissolved hydrogen resides at either NILS or trap sites and the concentration of hydrogen at these two sites is always in local equilibrium. The hydrogen in NILS is influenced by hydrostatic stress σ_h [17]. On the other hand, the hydrogen concentration in the trap sites depends on trap site density (i.e. number of traps per unit volume). This density is dependent on local equivalent plastic strain ϵ_p; the dependence is shown experimentally by Kumnick and Johnson [8]. Thus, the total hydrogen concentration and hence the damage to material is dependent on levels of both σ_h and ϵ_p.

Although both σ_h and ϵ_p are considered to have influence on HASCC, certain modelling [15, 16] have assumed that, for an elastic-plastic material under moderate to strong levels of ϵ_p, the plastic strain plays a substantially dominant role in determination of hydrogen distribution near the crack tip and the effect of σ_h may be neglected. This assumption simplifies a computational study. However, hydrostatic stress may become an important factor in situations where plastic strain levels are sufficiently small. The present study focuses on such situations.

In the present work, stable crack growth through a compact tension specimen of structural steel subjected to rising rate of displacement or load has been modelled using HCDCZM under HASCC conditions in simulated sea water environment. The crack growth has been simulated using a finite element code ABAQUS® (version 6.6)[1] and a CZM based element type

COH2D4. The variation of modified crack opening displacement against crack length is predicted using HCDCZM and these results for the three loading rates, where ϵ_p ranges from low to moderate, are compared with the experimental data of Scheider et al. [16] as well as the previous work of the authors where the effect of hydrostatic stress was ignored [15]. The magnitude of plastic strain below which the effect of hydrostatic stress becomes significant is indicated; this finding can serve as a guideline for future HASCC studies.

2. HYDROGEN CONCENTRATION DEPENDENT COHESIVE ZONE MODEL (HCDCZM)

The HCDCZM deals with representation of diffusion of hydrogen along crack front and hydrogen assisted stable crack growth. These two processes are interdependent. The presence of diffused hydrogen lowers the cohesive strength of material and promotes faster growth of crack. The propagation of crack, in turn, changes the distribution of hydrogen, stresses and strains, which leads to furtherance of diffusion. In the present study diffusion solution is obtained by a numerical solution to the governing differential equation and the crack growth is analysed by finite element based CZM.

2.1. Diffusion of hydrogen

The hydrogen available in the environment either directly or generated through corrosion reaction enters into the material by diffusion process. The hydrogen already inside the material is also driven towards regions of high stress and strain due to difference in chemical potential. The total hydrogen concentration C_{tot} at any point inside material is sum of concentration C_L in NILS and C_T in traps. C_L and C_T are considered to be always in equilibrium as per Oriani's law [13].

$$C_T = \frac{K\left(\frac{\alpha N_T}{\beta N_L}\right) C_L}{1 + \left(\frac{K}{\beta N_L}\right) C_L} \tag{1}$$

where trap equilibrium constant $K = 2.7977 \times 10^{10}$ (at 300 K), α represents number of hydrogen atom sites per trap, β is number of NILS per solvent atom and β=6 for iron considering tetrahedral site occupancy, N_L (=8.46×10^{28}) atoms/m^3 denotes number of solvent lattice atoms per unit volume [17, 18] and the trap density N_T measured in number of traps per unit volume is obtained in terms of equivalent plastic strain ϵ_p. α=1 is assumed in the present study [17]. The experimental data of N_T vs. ϵ_p obtained by Kumnick and Johnson [8] is fitted [7] as $\log N_T = 23.26 - 2.33e^{-5.5\epsilon_p}$. All data correspond to iron-hydrogen system.

The diffusion of hydrogen through metal is governed by a partial differential equation [18]:

$$\frac{\partial C_L}{\partial t} = \nabla\left(D_{eff}\nabla C_L\right) - \nabla\left(\frac{D_{eff}V_H}{RT}C_L\nabla\sigma_h\right) - f\left(\dot{\epsilon_p}\right) \tag{2}$$

where C_L is hydrogen concentration in NILS, D_{eff} is effective diffusivity of material, V_H is partial molar volume of hydrogen in metal (2×10^3 mm^3/mol for iron), R is universal gas constant (8.3144 J/mol-K), T is absolute temperature in °K. The last term $f\left(\dot{\epsilon_p}\right)$ was introduced by Krom et al. [7] to account for the effect of plastic strain rate. This term is not included in the

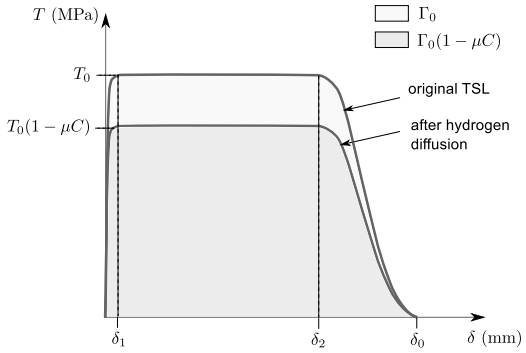

Figure 1. Concentration dependent traction separation law and effect of strength reduction factor μ [15].

present study. Eq. (2) is solved numerically to obtain transient hydrogen distribution along the crack line.

2.2. Crack propagation

In CZM approach, the behaviour of material during crack propagation is defined by the TSL. The damage to material is represented by any two of the three parameters of TSL: cohesive energy Γ_0, cohesive strength T_0 and critical separation δ_0. The shape of TSL is chosen as per the degree of plasticity of material. In this paper a trapezoidal TSL (Figure 1) considered by Scheider et al. [16] has been selected.

$$T = T_0(1-\mu C)\begin{cases} 2\left(\frac{\delta}{\delta_1}\right) - \left(\frac{\delta}{\delta_1}\right)^2, & \delta < \delta_1, \\ 1, & \delta_1 < \delta < \delta_2, \\ 2\left(\frac{\delta-\delta_2}{\delta_0-\delta_2}\right)^3 - 3\left(\frac{\delta-\delta_2}{\delta_0-\delta_2}\right)^2 + 1, & \delta_2 < \delta < \delta_0. \end{cases} \tag{3}$$

where $\delta_1 = 0.05\delta_0$ and $\delta_2 = 0.65\delta_0$. The strength reduction factor μ links directly the rise in normalised hydrogen concentration C and gives rise to a drop in cohesive strength T_0. In a sense it represents the effects of HEDE mechanism in the damage process. The hydrogen concentration C is normalised as $C = \frac{(C_{tot})}{(C_{tot})_{env}}$, where (C_{tot}) and $(C_{tot})_{env}$ are respectively the hydrogen concentrations in material and environment. This approach eliminates the need to measure $(C_{tot})_{env}$ which will be a difficult task.

3. CRACK GROWTH IN COMPACT TENSION SPECIMEN

The HCDCZM has been implemented here to model mode-I stable crack growth through a compact tension (CT) specimen. Both diffusion and crack propagation processes are integrated for better speed and accuracy of computation.

The data employed for mode-I stable crack growth in high strength low alloy structural steel (FeE690T) correspond to the experimental data of Dietzel and Pfuff [3] and Scheider et al. [16]. The CT specimens were 40 mm wide, 19 mm thick and pre-cracked to an initial crack length to width ratio a_0/W = 0.55. The tests were conducted both in laboratory air and simulated sea water environment. During the sea water tests hydrogen evolution was promoted

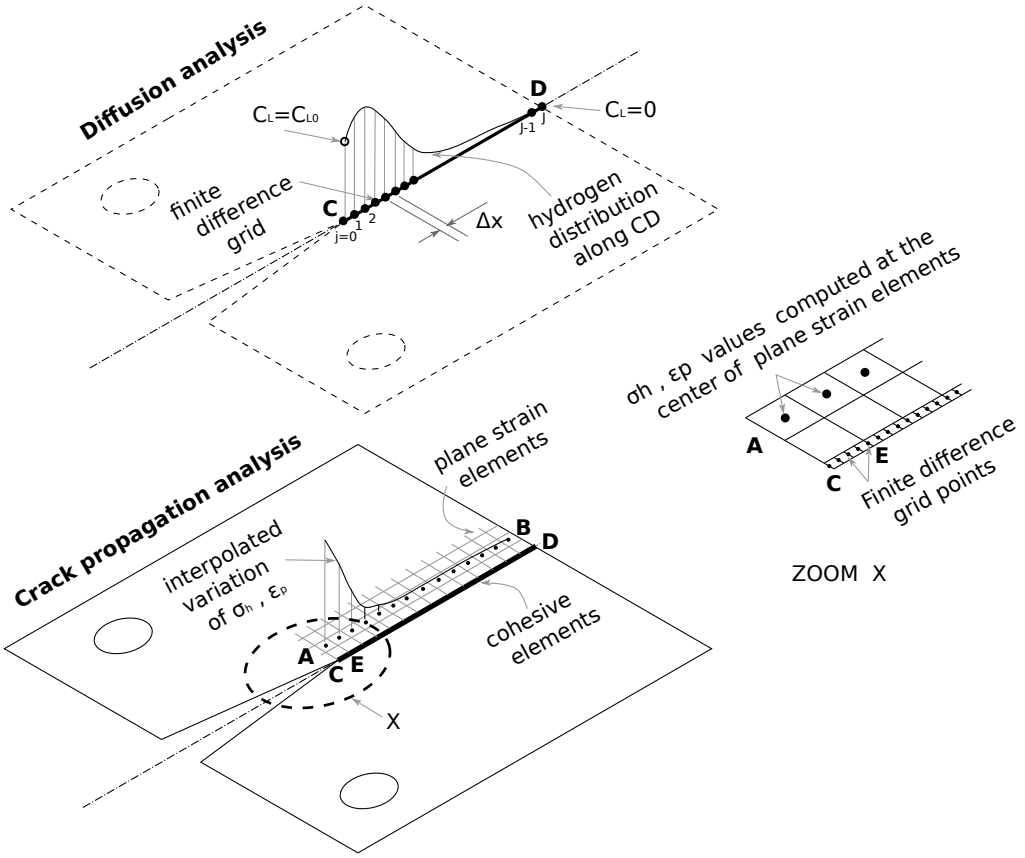

Figure 2. Finite difference scheme used in HCDCZM.

by cathodic charging. The material yield strength σ_y = 695 MPa and ultimate strength σ_u = 820 MPa. The stress-strain data of material is identical to the one used by Scheider et al. [16].

The tests under HASCC condition were performed at three rates of displacement loading: 0.001, 0.01 and 0.1 mm/h. The experimental results were presented as R-curves generated in terms of δ_5 vs. Δa, where δ_5 is the modified crack opening displacement [6].

$$\delta_5 = \frac{K^2(1-\nu^2)}{2\sigma_y E} + \frac{0.6\Delta a + 0.4(W-a_0)}{0.6(a_0+\Delta a) + 0.4W + z}\mathrm{v}_{pl} \tag{4}$$

where K is mode I stress intensity factor, E is modulus of elasticity, ν is Poisson's ratio, a_0 is initial crack length, Δa is crack extension, W is width of specimen, v_{pl} is plastic portion of the crack mouth opening displacement and z is the distance between the load-line and the actual measuring position for v.

3.1. Finite difference solution to the diffusion equation

The governing equation of diffusion, Eq. (2), is non-linear in the presence of the time-dependent term σ_h. A closed form solution to this equation such as the one obtained by Olden et al. [11] and Raykar et al. [15] is not possible. A numerical solution using finite difference method has been considered. It has been shown [15] that one dimensional solution to diffusion equation gives sufficiently accurate hydrogen distribution for the purpose of predicting stable crack growth; one dimensional solution to diffusion along the crack extension line has only

been considered. Eq. (2) can be rewritten for one dimension as follows.

$$\frac{\partial C_L}{\partial t} = D_{eff}\frac{\partial^2 C_L}{\partial x^2} - E_H\frac{\partial C_L}{\partial x}\frac{\partial \sigma_h}{\partial x} - E_H C_L\frac{\partial^2 \sigma_h}{\partial x^2} \tag{5}$$

where x is the distance from the crack tip along the crack path and

$$E_H = \frac{D_{eff}V_H}{RT}. \tag{6}$$

The effective diffusivity of material D_{eff} is assumed to be constant and equal to the value used in the previous study [15]. At $t = 0$, $C_L = 0$, i.e. complete absence of hydrogen is assumed across entire crack path. The boundary conditions are: for $t \geqslant 0$, $C_L = C_{L0}$ at the crack tip and for $t > 0$, $C_L = 0$ at the far end D of crack path (Figure 2). C_{L0} is the concentration of hydrogen in environment. C_{L0} is assumed to be equal to the stress free equilibrium solubility of hydrogen in iron at 300 K, i.e. 2.084×10^{21} atoms/m^3 [17]. The equilibrium concentration in traps C_{T0} corresponding to C_{L0} is calculated from Eq. (1) as 8.4379×10^{20} atoms/m^3.

The finite difference representation of Eq. (5) is obtained [14] using Crank-Nicholson scheme.

$$\begin{aligned}
&\frac{(C_L)_j^{n+1} - (C_L)_j^n}{\Delta t} \\
&= \frac{D_{eff}}{2}\left[\frac{\left[(C_L)_{j-1}^{n+1} - 2(C_L)_j^{n+1} + (C_L)_{j+1}^{n+1}\right] + \left[(C_L)_{j-1}^{n} - 2(C_L)_j^{n} + (C_L)_{j+1}^{n}\right]}{(\Delta x)^2}\right] \\
&\quad - \frac{E_H}{2}\left[\frac{\left[(C_L)_{j+1}^{n+1} - (C_L)_{j-1}^{n+1}\right] + \left[(C_L)_{j+1}^{n} - (C_L)_{j-1}^{n}\right]}{2(\Delta x)}\right]\left[\frac{(\sigma_h)_{j+1}^n - (\sigma_h)_{j-1}^n}{2(\Delta x)}\right] \\
&\quad - \frac{E_H}{2}\left[(C_L)_j^{n+1} + (C_L)_j^n\right]\left[\frac{(\sigma_h)_{j-1}^n - 2(\sigma_h)_j^n + (\sigma_h)_{j+1}^n}{(\Delta x)^2}\right]
\end{aligned} \tag{7}$$

where $(C_L)_j^n$ is magnitude of C_L at time step n; $j = 0, 1, 2, ..., J$ are grid points; Δt is the time interval between step $(n+1)$ and n; Δx is the distance between grid points which is kept equal to the cohesive element size used in the crack propagation analysis.

The diffusion and crack propagation analyses start at the same time and are repeated with the same time interval Δt. The selection of Δt is based on a numerical stability criterion [14] for the diffusion solution.

$$\Delta t \leqslant \frac{(\Delta x)^2}{2D_{eff}}. \tag{8}$$

The values of σ_h and ϵ_p and current crack length required for solving Eqn.(7) are computed through the crack propagation analysis and passed on to diffusion analysis (Figure 2). Upon detection of increase in the crack length, the number of active grid points are correspondingly reduced to $j = i, i+1, ..., J$ where i is the grid point corresponding to the new position of crack tip and the boundary condition $C_L = C_{L0}$ is shifted to grid point i.

Starting with the specified initial condition, values of C_L at time step $(n+1)$ can be obtained in terms of C_L at time step n through Eq. (7). This equation is applied at each of the inner grid points $j = (i+1)$ to $(J-1)$ and after rearrangement of terms in Eq. (7) this procedure

gives a set of $(J-i-1)$ linear equations.

$$(-\alpha_1+\beta_1)(C_L)_{j-1}^{n+1}+(1+2\alpha_1-\gamma_1)(C_L)_j^{n+1}+(-\alpha_1-\beta_1)(C_L)_{j+1}^{n+1}$$
$$=(\alpha_1-\beta_1)(C_L)_{j-1}^{n}+(1-2\alpha_1+\gamma_1)(C_L)_j^{n}+(\alpha_1+\beta_1)(C_L)_{j+1}^{n} \quad (9)$$

where

$$\alpha_1=\frac{D_{eff}\Delta t}{2(\Delta x)^2} \quad (10)$$

$$\beta_1=\frac{E_H\Delta t}{8(\Delta x)^2}[(\sigma_h)_{j+1}^n-(\sigma_h)_{j-1}^n] \quad (11)$$

$$\gamma_1=\frac{E_H\Delta t}{2(\Delta x)^2}[(\sigma_h)_{j-1}^n-2(\sigma_h)_j^n+(\sigma_h)_{j+1}^n] \quad (12)$$

$$j=(i+1),2,3,...,(J-1)$$

These simultaneous equations are solved to obtain $(C_L)_j^{n+1}$ at the grid points j and this is repeated in every time step.

3.2. Finite element (FE) based CZM of crack propagation

The CT specimen is discretised using 4 noded quadrilateral plane strain elements (Figure 3) of 0.1 mm size around the crack extension line. This element size was arrived at by trial and error using δ_5 vs. Δa results of Scheider et al. [16] for test in air. The cohesive elements of zero height and 0.025 mm width are placed along the crack path. The FE mesh is identical to the one used by Raykar et al. [15]. The node positions of cohesive elements are identical to the spacing of grid points used in the finite difference solution. The node at the centre of bottom pin is held fixed while the centre of the top pin is subjected to the displacement load. The TSL for cohesive elements uses $T_0=2390$ MPa and $\delta_0=0.016$ mm; these values were determined [15] by matching the simulation results with the experimental δ_5 vs. Δa curve for the test in air.

The coupled diffusion and finite element analysis is facilitated through user subroutine USDFLD of ABAQUS®. This routine computes the latest value of hydrogen concentration C_L on grid along CD (Figure 2) using Eq. (7). The values of σ_h and ϵ_p required at the same grid points are obtained through interpolation of the average values at centre of the plane strain elements along AB. The spacing between AB and CD is neglected for this purpose. It may be noted that there are four grid points over each element span, e.g. CE. The values at the row of elements between AB and CD are not considered to avoid errors due to proximity of this row to the cohesive elements along CD. The term C used in Eq. (3) for modification of TSL is calculated as follows.

$$C=\frac{(C_L+C_T)}{(C_{L0}+C_{T0})} \quad (13)$$

The C_T is calculated from C_L using Eq. (1). The TSL is updated according to C at each integration point of the cohesive elements. The computation of damage to cohesive elements during crack propagation simulation proceeds with the updated TSL.

The load line displacement is obtained through the finite element based CZM analysis and the corresponding δ_5 is calculated using Eqn. (4) with $z=0$.

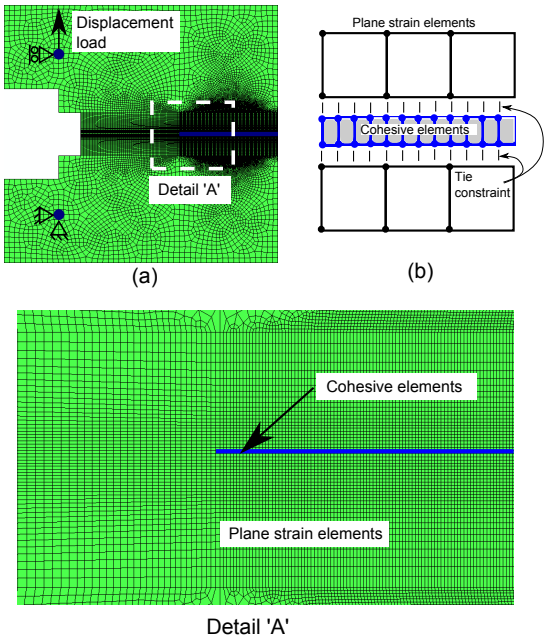

Figure 3. Finite element discretisation [15]. (a) FE mesh and boundary conditions (b) schematic arrangement of cohesive elements.

4. RESULTS AND DISCUSSION

The prediction of stable crack growth using HCDCZM is highly dependent on the selection of two modelling parameters: effective diffusivity D_{eff} and strength reduction factor μ. The parameter D_{eff} has been computed in a previous work [15] as 5.5×10^{-6} mm^2/s. This value lies within the experimentally measured [4] range of 2.0×10^{-5} to 8.0×10^{-7} mm^2/s; the same has been found suitable in the present study as well. The parameter μ represents extent of drop in strength corresponding to a unit hydrogen concentration. The values of μ corresponding to the three loading rates have been obtained (Table 1) by matching the predicted results of δ_5 vs. Δa with the experimental data of Scheider et al. [16]. Table 1 shows that μ is highest for the slowest loading rate. This variation of μ is consistent with the findings of Krom et al. [7] wherein the damage during HASCC is shown to be dependent on plastic strain rate: the lowest plastic strain rates lead to the highest drop in strength. The lowest plastic strain rates occur at the slowest loading rates and the corresponding value of μ is the highest. Figure 4 shows a comparison of predicted and experimental δ_5 vs. Δa variation. The results due to an earlier study [15] are also included in Figure 4. The predicted results of the present study which includes the effects due to σ_h, are in agreement with the experimental data. Notably, it is also close to the results obtained without considering the effect of σ_h [15].

Corresponding to $\Delta a = 0.025$ and $\Delta a = 1.0$ mm, the variations of C_L, C_T, σ_h and ϵ_p with distance from the crack tip for the three loading rates (0.001, 0.01 and 0.1 mm/h) are shown in Figures 5, 6 and 7 respectively. There is resemblance between the distributions of C_L and σ_h on one hand, and C_T and ϵ_p on the other. This clearly indicates the influence of distribution of σ_h on C_L and ϵ_p on C_T. The distribution of total hydrogen concentration C is shown in Figures 8, 9 and 10 for the three rates respectively. These figures also include the results of earlier study [15] where the effects of σ_h on diffusion were neglected. In the present study, the maximum

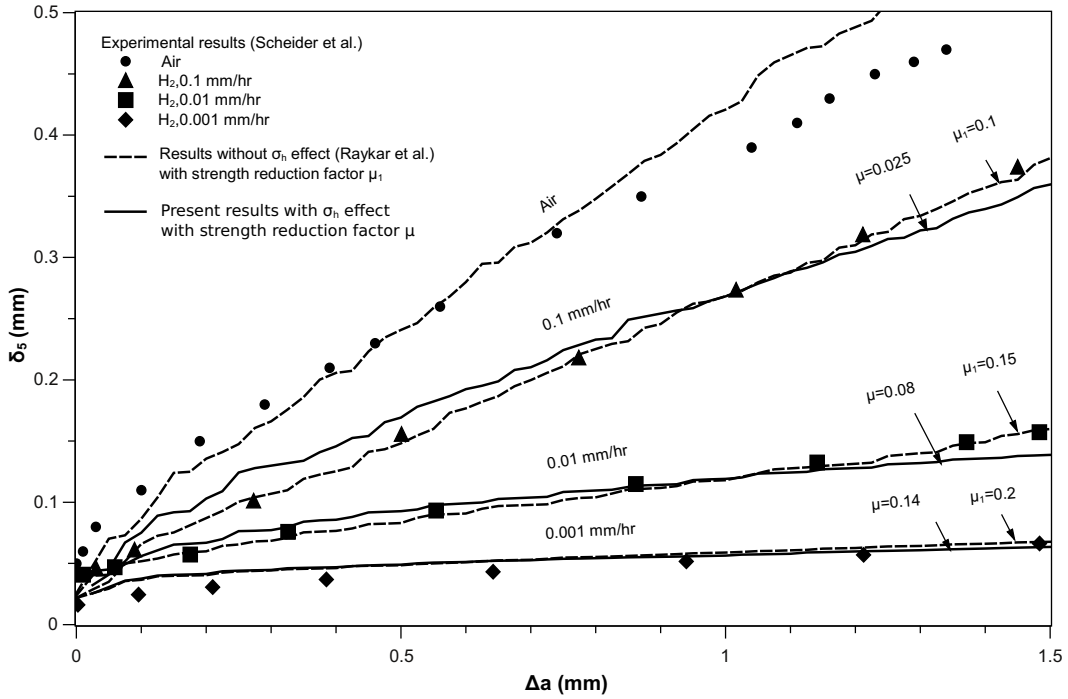

Figure 4. Comparison of results with and without hydrostatic stress σ_h effect.

value of hydrogen concentration occurs at a finite distance ahead of crack tip and it has values higher than 1. The peak location varies with loading rates and it occurs at a point closer to the crack tip at higher loading rates. Further the hump in profile of C is the narrowest at the highest loading rate.

The average concentration C^p_{avg} of hydrogen in the three cases of loading rates were evaluated by numerically integrating the plot of C vs. distance up to 1 mm ahead of the crack tip. The same data C^e_{avg} was also computed in the case of earlier study. These two sets of average C are compared in Table 2. The average hydrogen concentration is always higher in the present study. Since higher levels of average C indicate a higher damage and perhaps more crack growth rate, to predict the same experimental variation δ_5 with Δa, it is necessary to keep the same extent of reduction in the strength of cohesive elements. That is, μC must be closer in the two cases. This calls for lowering of μ's in the present study matching the higher levels of hydrogen concentrations. μ's obtained through the numerical studies (Table 2) tallies almost exactly with this expectation except in the case of highest loading rate.

The total hydrogen concentration C in the case of first two loading rates (0.001 and

Table 1. Values of strength reduction factor μ.

	Rate of loading (mm/h)		
	0.001	0.01	0.1
μ^p with σ_h effect (present study)	0.140	0.080	0.025
μ^e without σ_h effect [15]	0.200	0.150	0.100

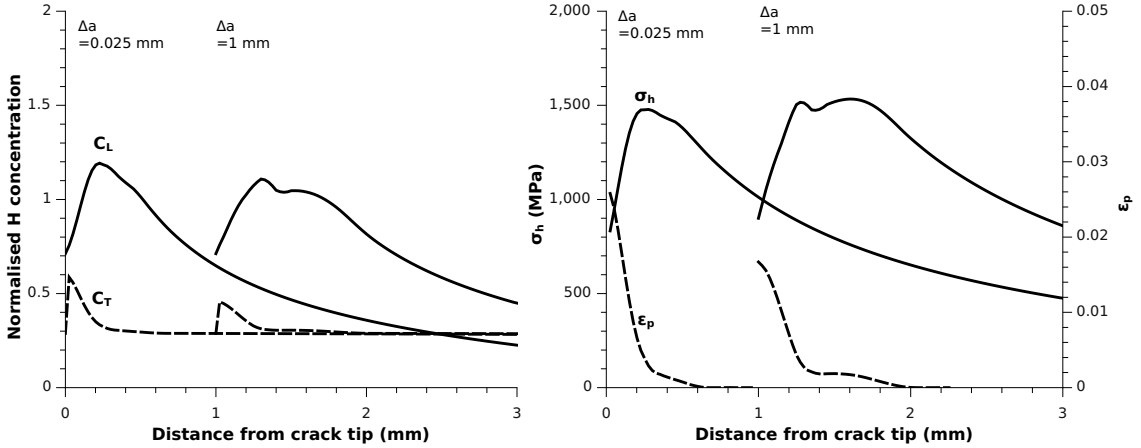

Figure 5. Variation of C_L, C_T, σ_h and ϵ_p near crack tip, rate of loading = 0.001 mm/h.

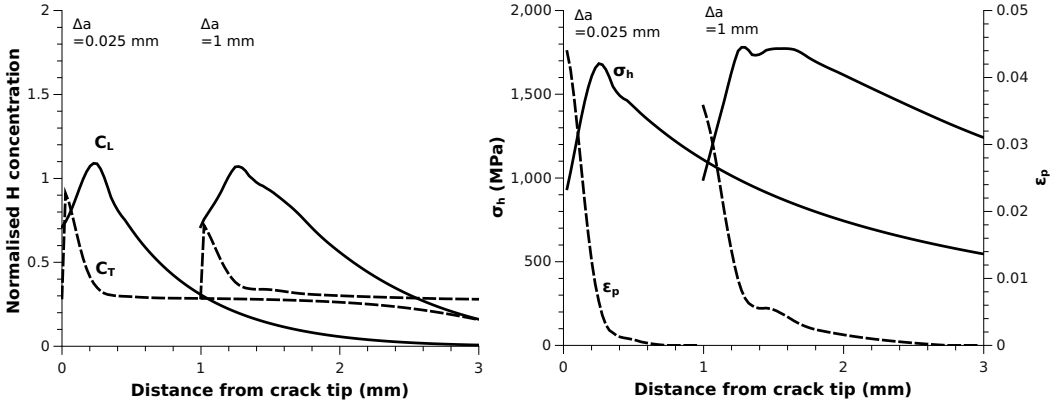

Figure 6. Variation of C_L, C_T, σ_h and ϵ_p near crack tip, rate of loading = 0.01 mm/h.

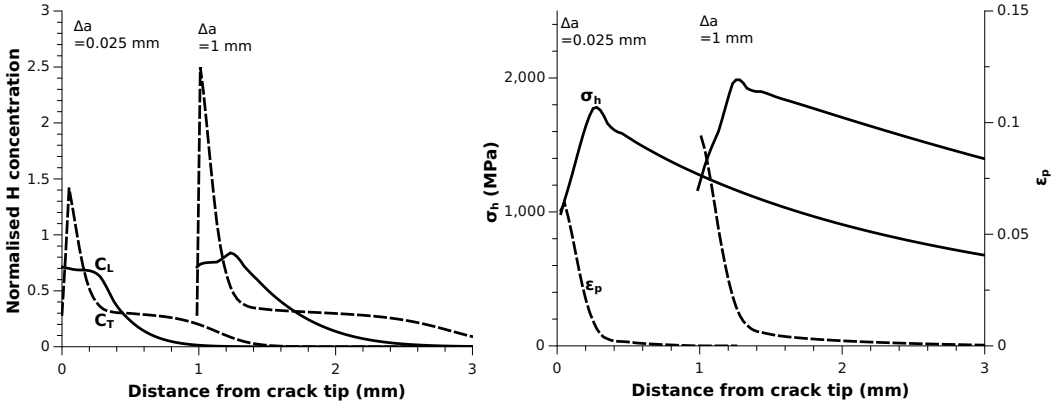

Figure 7. Variation of C_L, C_T, σ_h and ϵ_p near crack tip, rate of loading = 0.1 mm/h.

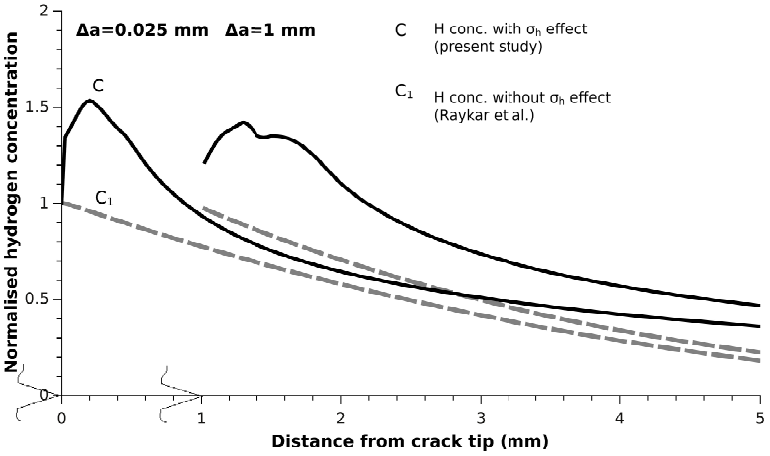

Figure 8. Comparison of C with and without σ_h effect for loading rate of 0.001 mm/h.

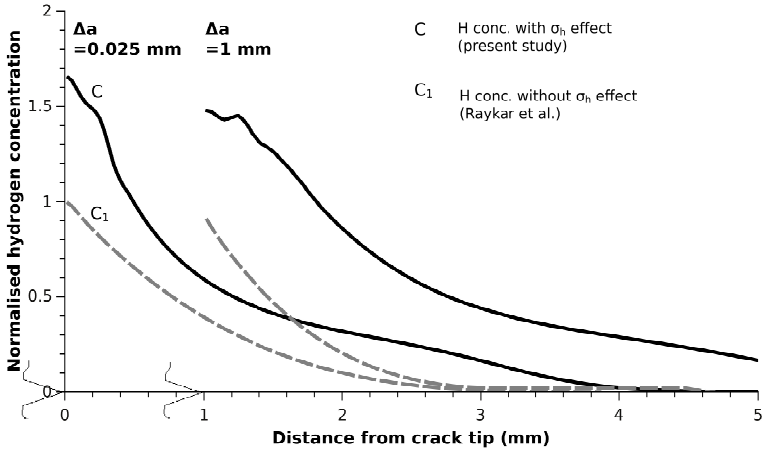

Figure 9. Comparison of C with and without σ_h effect for loading rate of 0.01 mm/h.

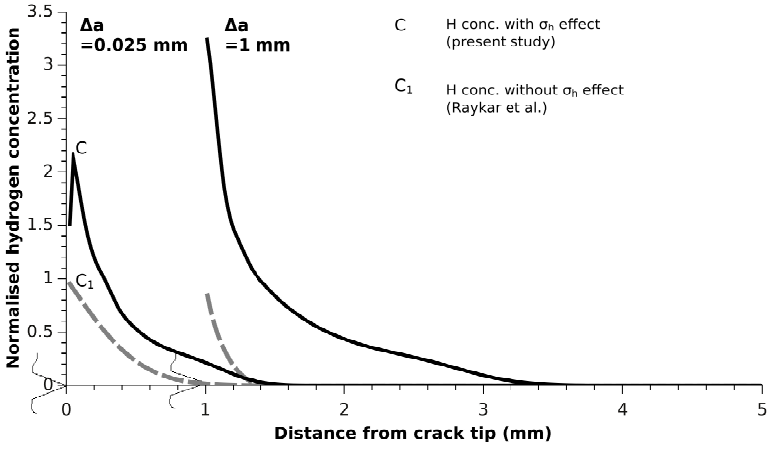

Figure 10. Comparison of C with and without σ_h effect for loading rate of 0.1 mm/h.

Table 2. Comparison of average hydrogen concentration C_{avg} and estimation of μ.

		Rate of loading (mm/h)		
		0.001	0.01	0.1
Earlier study [15]	C^e_{avg}	0.87	0.64	0.30
Present study	C^p_{avg}	1.24	1.01	0.70
Earlier study [15]	Damage $D_H = \mu^e \times C^e_{avg}$	0.174	0.096	0.030
Present study	Estimated $\mu = D_H / C^p_{avg}$	0.140	0.095	0.043
	Selected μ^p	0.140	0.080	0.025

0.01 mm/h) is dominated by the distribution of C_L than C_T. The maximum value of equivalent plastic strain $(\epsilon_p)_{max}$ near the crack tip at Δa = 1 mm for these two cases are 0.017 and 0.036 respectively. The total hydrogen concentration in the third case of loading rate (0.1 mm/h, $(\epsilon_p)_{max}$ = 0.099) is dominated by that of C_T. This means that the total concentration distribution in the third case, where $\epsilon_p > 0.05$, is dominated by the equivalent plastic strain ϵ_p distribution than σ_h distribution. Nevertheless, the average concentration C^p_{avg} in the third case of loading rate too is higher than in the corresponding case of the earlier study [15]. This called for lowering of μ in this case too for the crack growth study.

5. CONCLUSIONS

The influence of hydrostatic stress σ_h on modelling of hydrogen assisted stress corrosion crack growth in structural steel can be addressed by HCDCZM model. Main observations from the present study are as follows.

(a) A close integration of finite difference based diffusion solution with the finite element based CZM approach for crack growth provides an equally stable and fast method for the modelling of HASCC as compared to an earlier study [15] based on an analytical solution to the diffusion equation.

(b) The present study with the inclusion of the effects of hydrostatic stress σ_h predicts the experimental crack growth behaviour [16] employing lower values of μ and the same value of D_{eff} as in the case of an earlier study with the exclusion of the effects of σ_h [15].

(c) The hydrogen concentration distribution C near the crack tip is observed to closely follow the variation of σ_h for lower range of equivalent plastic strain ϵ_p and it gradually reduces as ϵ_p increases. The peak of hydrogen distribution is always located away from the crack tip when the influence of σ_h is significant; the peak occurs at the crack tip if this influence is ignored. The influence of hydrostatic stress on the hydrogen concentration distribution near the crack tip is observed to be significant for $\epsilon_p < 5\%$.

(d) The hydrogen concentrations have higher average values ahead of the crack tip in the present study as compared to the earlier study. The damage parameter μ is reduced in

the present study so as to keep μC almost at the same level to get a good match between the predicted and experimental results.

(e) There is a possibility of predicting the experimental data on crack growth reasonably closely without going for accounting the hydrostatic stress effects in the diffusion analysis.

6. REFERENCES

[1] ABAQUS, *Version 6.6, Analysis users' manual*. ABAQUS Inc., 2006.

[2] Barenblatt G.I., "The mathematical theory of equilibrium cracks in brittle fracture". *Advanced Applied Mechanics*, 7, 55–129, 1962.

[3] Dietzel W., Pfuff M., "Effect of deformation rates on hydrogen embrittlement". In A.W. Thompson, N. Moody (eds.), "Hydrogen effects in materials", 303–311, Minerals, Metals & Materials Soc (TMS), 1996.

[4] Dietzel W., Pfuff M., Juilfs G., "Hydrogen permeation in plastically deformed steel membranes". *Materials Science*, 42, 78–84, 2006.

[5] Gangloff R.P., "Hydrogen Assisted Cracking in High Strength Alloys". In "Comprehensive Structural Integrity, Environmentally-Assisted Fracture", volume 6, Elsevier, Oxford, 2003.

[6] Hellmann D., Schwalbe K.H., "On the experimental determination of CTOD based R-curves". In K.H. Schwalbe (ed.), "The crack tip opening displacement in elastic-plastic fracture mechanics", Springer, Heidelberg, 1986.

[7] Krom A.H.M., Koers R.W.J., Bakker A., "Hydrogen transport near a blunting crack tip". *Journal of the Mechanics and Physics of Solids*, 47, 971–992, 1999.

[8] Kumnick A., Johnson H., "Deep trapping states for hydrogen in deformed iron". *Acta Metallurgica*, 28(1), 33 – 39, 1980.

[9] Liang Y., Sofronis P., "Toward a phenomenological description of hydrogen-induced decohesion at particle/matrix interfaces". *Journal of the Mechanics and Physics of Solids*, 51(8), 1509 – 1531, 2003.

[10] Lynch S., "Progress towards understanding mechanisms of hydrogen embrittlement and stress corrosion cracking". In "NACE - International Corrosion Conference Series", 074931 – 0749355, NACE International, 2007.

[11] Olden V., Thaulow C., Johnsen R., "Modelling of hydrogen diffusion and hydrogen induced cracking in supermartensitic and duplex stainless steels". *Materials and Design*, 29, 1934–1948, 2008.

[12] Olden V., Thaulow C., Johnsen R., Ostby E., Berstad T., "Application of hydrogen influenced cohesive laws in the prediction of hydrogen induced stress cracking in 25%Cr duplex stainless steel". *Engineering Fracture Mechanics*, 75, 2333–2351, 2008.

[13] Oriani R.A., "The diffusion and trapping of hydrogen in steel". *Acta Metallurgica*, 18, 147–157, 1970.

[14] Press W.H., Teukolsky S.A., Vetterling W.T., Flannery B.P., *Numerical recipes in FORTRAN, The art of Scientific Computing*. Cambridge University Press, 2nd edition, 1998.

[15] Raykar N.R., Maiti S.K., R.K. Singh Raman, "Modelling of Mode-I Stable Crack Growth under Hydrogen Assisted Stress Corrosion Cracking". *Engineering Fracture Mechanics*, 78, 3153–3165, 2011.

[16] Scheider I., Pfuff M., Dietzel W., "Simulation of hydrogen assisted stress corrosion cracking using the cohesive model". *Engineering Fracture Mechanics*, 75, 4283–4291, 2008.

[17] Sofronis P., McMeeking R., "Numerical analysis of hydrogen transport near a blunting crack tip". *Journal of the Mechanics and Physics of Solids*, 37(3), 317 – 350, 1989.

[18] Taha A., Sofronis P., "A micromechanics approach to the study of hydrogen transport and embrittlement". *Engineering Fracture Mechanics*, 68(6), 803 – 837, 2001.